

Pervaporation-driven electrokinetic energy harvesting using poly(dimethylsiloxane) microfluidic chips

Hrishikesh Pingulkar,¹ Cédric Ayela,² and Jean-Baptiste Salmon¹

¹CNRS, Syensqo, LOF, UMR 5258, Université de Bordeaux, 178 av. Schweitzer, 33600 Pessac, France.

²Université de Bordeaux, IMS, CNRS, Bordeaux INP, UMR 5218, 33607 Pessac, France.

Electrokinetic energy harvesting from evaporation-driven flows in porous materials has recently been the subject of numerous studies, particularly with the development of nanomaterials with high conversion efficiencies. The configuration in which the energy conversion element is located upstream of the element which passively drives the evaporative flow has rarely been studied. However, this configuration offers the possibility of increasing the harvested energy simply by increasing the evaporation surface area and/or the hydraulic resistance of the energy conversion element. In this work, we investigate this configuration with poly(dimethylsiloxane) (PDMS) chips playing the role of *artificial leaves* driving a pervaporation-induced flow through a polystyrene colloid plug in a submillimetre tube for the energy conversion. With an appropriate design of the venation of the PDMS leaves, we report the first experimental evidence of electrokinetic energy conversion from pervaporation-induced flows, which increases with the pervaporation area. We also provide new insights by demonstrating that this increase is limited by cavitation within the PDMS leaves, which occurs systematically as soon as the water pressure inside the leaf reaches $P_{\text{leaf}} \simeq 0$ bar. Whatever the cavitation threshold, this phenomenon imposes an intrinsic limit on this configuration, underlining the need for innovative strategies to improve the harvesting of electrokinetic energy by evaporation.

I. INTRODUCTION

Since Osterle's pioneering work¹, electrokinetic (EK) mechanisms for converting mechanical energy into electrical energy, based on the concepts of streaming currents and streaming potentials in pressure-driven flows, have been well established both experimentally and theoretically²⁻⁷. Most of these studies focus on the EK energy conversion efficiency, because the mechanical input energy associated with the flow is imposed externally in the intended applications (hydrostatic pressure).

More recently, it has been shown that water evaporation from saturated porous media can also be used to harvest electrical energy using the same EK mechanisms^{8,9}. These EK mechanisms also partly explain the harvesting of electrical energy from ambient humidity, as recently demonstrated using various specific nanoporous materials, commonly known as *moist-electric generators*¹⁰⁻¹². Evaporation-induced flows occur spontaneously and continuously because they are passively driven by chemical potential gradients, thus opening up new application possibilities. These studies are part of a more general theme that considers the natural evaporation of water, as well as the ambient moisture, as potentially reliable sources of renewable energy¹²⁻¹⁴. To date, several experimental demonstrations of EK energy conversion from water evaporation in saturated porous media have been reported, involving energy conversion materials as diverse as cellulose-based paper¹⁵ and textiles¹⁶, nanoporous membranes¹⁷, glass microchannels^{18,19}, clay minerals²⁰, carbonized biomass²¹, but also electronically conducting and carbon-based nanomaterials²²⁻²⁷ for which the energy conversion mechanisms involve more subtle effects²⁸. Most of these studies are mainly proofs of concept focusing on EK energy conversion performance via the development of new materials.

Yaroshchuk recently carried out a critical review of this rapidly expanding field²⁹, and pointed out that, to date, there

has been no satisfactory quantitative comparison with theoretical models, even in the case of standard EK mechanisms, notably due to the lack of precise experimental characterisation of the electrochemical collection of the streaming currents by the electrodes. Yaroshchuk also identified that the configuration in which the element driving the flow is separate from the EK conversion offers better optimisation possibilities. This configuration is shown in Fig. 1 thanks to the analogy with evapo-transpiration that continuously transports water in plants, from the soil to the leaves to maintain their hydration^{30,31}. In this illustration, evaporation from the leaves drives a flow at a rate Q through an EK conversion element (*trunk*) which harvests electrical power $\mathcal{P}_e = VI$ from the input mechanical power $\mathcal{P}_h = \Delta P Q$ with an efficiency $\varepsilon = \mathcal{P}_e / \mathcal{P}_h$, I being the current collected in a parallel load resistance R_L , V the associated electric potential, and ΔP the pressure drop across the EK conversion element. As pointed out by Yaroshchuk²⁹, it is the flow rate Q and the hydraulic resistance $R_h = \Delta P / Q$ of the EK conversion element that are the relevant parameters in such passive configurations for significantly increasing the electrical power, as $\mathcal{P}_e = \varepsilon R_h Q^2$. To our knowledge, this configuration has only been explored by a few groups with the emphasis on the possible applications^{8,16,18}.

The aim of our work is firstly to provide a proof of concept of this configuration using *artificial leaves* made in poly(dimethylsiloxane) (PDMS), see Fig. 2, and then to study its intrinsic limitation due to cavitation, similar to the embolisms observed in trees during periods of intense drought³⁰. PDMS not only enables the rapid prototyping of chips using soft lithography, but is also slightly permeable to water. Water molecules from microchannels in a PDMS chip thus solubilise in the matrix, diffuse, and evaporate into ambient air, a process known as *pervaporation*. Due to mass conservation, pervaporation inevitably induces flows in PDMS chips, at rates Q of the order of a few nL h^{-1} for a single channel of a few centimetres long^{32,33}. Although these flows are often negligible

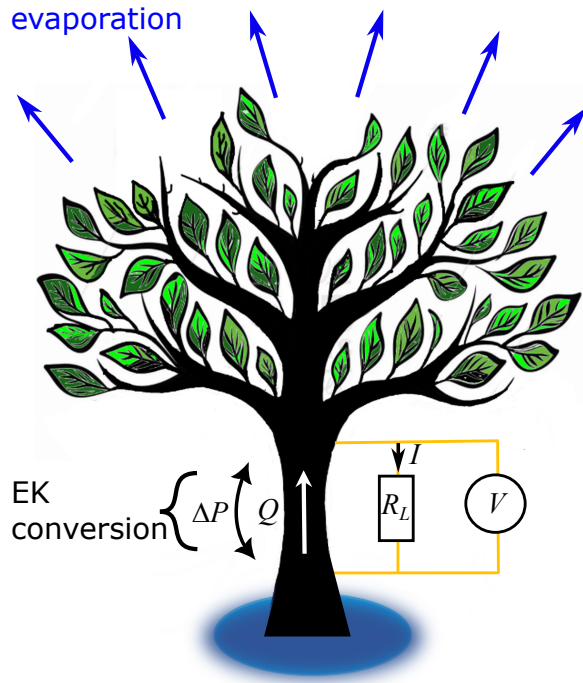


FIG. 1. Illustration of evaporation-driven EK energy harvesting in a configuration for which the evaporation surface (*leaves*) and the EK conversion element (*trunk*) are separate and in series. By analogy with evapo-transpiration in plants, evaporation induces a flow at a rate Q , associated to a pressure drop ΔP across the EK conversion element. A fraction of the streaming current is collected in a load resistance R_L placed in parallel.

for the majority of microfluidic studies, they have also found numerous applications³⁴. In the present work, we optimized the cm^2 channel network of the PDMS leaves³⁵ to achieve pervaporation-driven flow rates up to $Q \simeq 20 \mu\text{L h}^{-1}$. For the EK conversion element, we followed the strategy proposed in Refs.^{36,37} and fabricated a plug of charged-stabilized colloids closely-packed upstream of a filter in a submillimetre-sized tube. Pressure-driven flow through this charged nanoporous medium then results in a streaming current that can be collected in an external electrical circuit. We finally tuned the hydraulic resistance R_h of the colloid plug to reach relatively large pressure drops $\Delta P = R_h Q$ from the pervaporation-driven flow rates, and hence a measurable output electrical power \mathcal{P}_e that varies with the area of the PDMS leaves. We nevertheless showed that this output energy is limited by cavitation in the PDMS leaves, as soon as the pressure drop reaches $\Delta P \simeq 1$ bar. Whatever the cavitation threshold that would be reached for any other microfluidic system, our results show that cavitation in the configuration shown in Fig. 1 possibly limits the strategy of increasing the evaporation surface to increase the energy harvested.

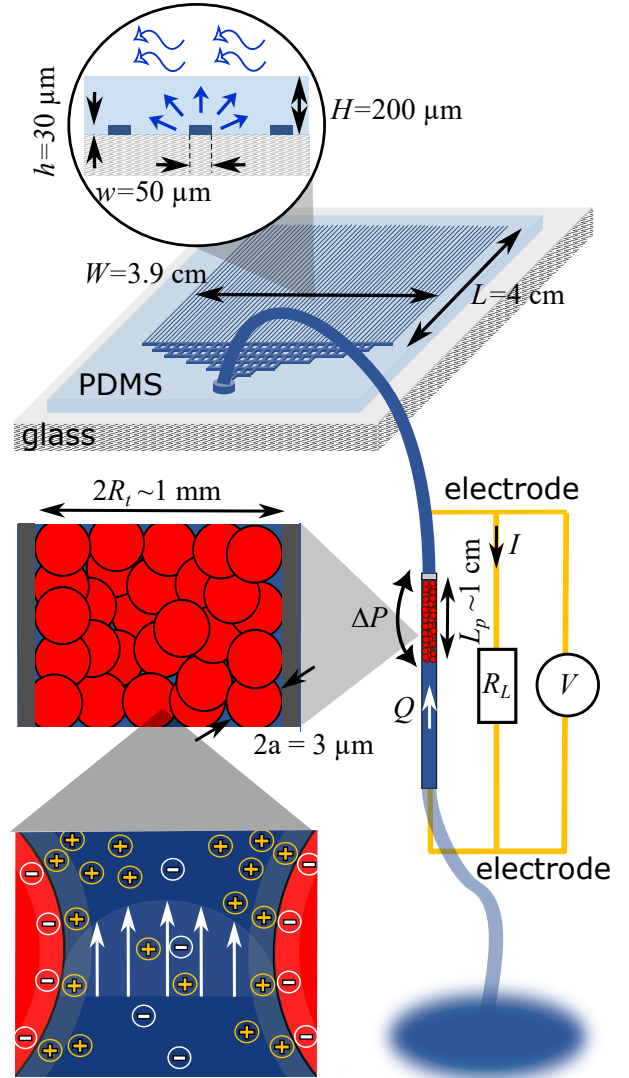


FIG. 2. EK energy harvesting from pervaporation-driven flows in a PDMS leaf. The EK conversion element consists of a plug of charged-stabilized colloids upstream of a filter fitted into a tube. Pervaporation in the PDMS leaf induces a flow rate Q and streaming currents through the interstices of the plug that are collected by electrodes in a load resistance R_L . The output electric power is $\mathcal{P}_e = VI$ and the input mechanical power is $\mathcal{P}_h = \Delta P Q$.

II. MATERIALS AND METHODS

A. Fabrication of PDMS leaves

Firstly, we used standard photolithography techniques to obtain a mold of microchannels with height $h = 30 \mu\text{m}$ on a silicon wafer (SU-8 photoresist). The design of the network of the channels is shown in the 3D view in Fig. 2 (see also Fig. S1 in Supplementary Material). It consists of $N = 79$ parallel dead-end channels of length $L = 4$ cm connected to a single inlet. The width of each channel is $w = 50 \mu\text{m}$, the center-

to-center distance between adjacent channels is $d = 500 \mu\text{m}$, leading to a width of $W = 3.9 \text{ cm}$ for the entire network.

We then used soft lithography techniques to make PDMS artificial leaves from this network of channels. More precisely, a PDMS layer of thickness $H \simeq 200 \mu\text{m}$ (Sylgard 184, curing agent/PDMS ratio: 1/10) is initially spin-coated onto the mold and then cross-linked at 65°C for a few hours. At the same time, a thicker PDMS structure ($\simeq 5 \text{ mm}$) with a hollow square cavity slightly larger than the area $L \times W$ of the channel network is made on a bare silicon wafer. This PDMS block with a frame-like structure is then peeled off from the wafer and bonded to the thin PDMS layer covering the channels using a plasma treatment. The assembly is then carefully peeled off from the wafer, punched to make the fluid inlet, and bonded to a glass slide using again a plasma treatment. The thick PDMS frame is essential not only to ensure the mechanical strength of the tube connected to the fluid inlet of the channels, but also to handle the thin cm^2 PDMS layer during the peeling step and avoid wrinkles that would trap air bubbles during the bonding step.

B. Electrical and flow measurements

Fluid pressure was controlled in the experiments described below using the Fluigent MCFS-EZ device, capable of imposing pressure differences of up to $\Delta P = 7 \text{ bar}$. Flow rates were measured using the flow units Fluigent S ($0 \pm 7 \mu\text{L min}^{-1}$) and XS ($0 \pm 1.5 \mu\text{L min}^{-1}$) depending on the flow rate range. Streaming potentials V were recorded using a digital multi-meter (Agilent, 34405A) with an internal impedance of $R_{\text{app}} = 10 \text{ M}\Omega$. The resistance R_{var} in parallel of the EK conversion was varied in the $R_{\text{var}} = 1 \Omega$ to $10 \text{ M}\Omega$ range using a decades resistance box (Centrad, DR07). In this range, the impedance of the multi-meter must be taken into account and the load resistance R_L in Fig. 2 is $R_L = R_{\text{var}} R_{\text{app}} / (R_{\text{var}} + R_{\text{app}})$. Local observations of the PDMS leaf were obtained using a stereomicroscope (Olympus SZX10) coupled with a sCMOS camera (Hamamatsu).

C. EK conversion element

We used polystyrene latex beads of mean diameter $2a = 3 \mu\text{m}$ (Sigma Aldrich, LB30, batch mass fraction 10%) as the building block of the colloidal plug of the EK conversion element shown in Fig. 3(a). We first prepared dispersions of known volume fraction ϕ_0 by dilution of the batch dispersion with deionised water, typically $\phi_0 = 5\%$. The particles are then accumulated by frontal filtration in a submillimetre-sized tube (inner diameter $2R_t$, ranging from 0.25 to 1 mm depending on the experiments, IDEX) upstream of a filter (porosity $0.5 \mu\text{m}$, IDEX, P-273x) nested in a fluidic T connector (PEEK, IDEX), see Fig. 3(a). More precisely, a given volume V_c of dispersion is injected into the tube, then filtered at a typical pressure of 6 bar with water upstream, while measuring simultaneously the flow rate. We consider that the colloidal plug is correctly formed as soon as the flow rate reaches a

steady value. The desired length L_p of the plug is estimated from mass conservation $\phi_0 V_c \simeq \pi R_t^2 L_p \phi_d$ assuming the particles are randomly close-packed ($\phi_d \simeq 0.64$), and also measured directly in the tube using a ruler.

To collect streaming currents, we used Ag/AgCl electrodes prepared from silver wires of diameter $500 \mu\text{m}$ (Sigma-Aldrich). Wires of 10 cm long are first rinsed with isopropanol to remove any surface contamination, then partially immersed in a 30% NaClO (Clorox bleach) solution for 30 min to chloride the silver wires. The prepared electrodes are then rinsed with isopropanol and deionised water and are embedded within the T connectors, as shown in Fig. 3(a). This configuration makes it easy to adjust the position of the electrodes, one upstream and close to the colloidal plug, the other downstream and close to the filter.

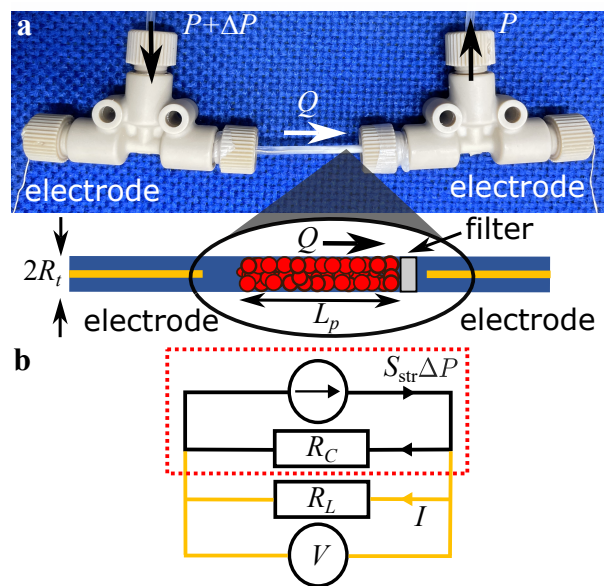


FIG. 3. EK conversion element. (a) Millifluidic assembly showing the colloidal plug upstream of a filter fitted into a tube of inner diameter $2R_t$ ranging from 0.25 to 1 mm depending on the experiments. Ag/AgCl electrodes located close to the plug and downstream of the filter are used to collect the current. ΔP is the pressure drop across the plug. (b) Equivalent circuit of the EK conversion element (red dotted rectangle) connected to a load resistance R_L (see text).

In our experiments, the colloidal particles are negatively charged so that the flow advects predominantly cations. Chloride ions are thus released at the right electrode in Fig. 3 (cathode) due to the transformation of AgCl into metallic Ag ($\text{AgCl(s)} + e^- \rightarrow \text{Ag(s)} + \text{Cl}^-$), while chloride ions are integrated in the left electrode in Fig. 3 (anode), therefore leading to a flux of electrons in the external electrical circuit from the anode to the cathode, see Ref.²⁹ for more information.

III. RESULTS AND DISCUSSION

A. Pervaporation-driven flows: from a single channel to parallel leaves

We first discuss the design and characterisation of the PDMS leaf illustrated schematically in Fig. 2, which passively drives a flow due to water evaporation in ambient air. Dollet *et al.* showed that the pervaporation-driven flow rate Q_i for a single dead-end channel of length $L \gg H \gg h$ is given by³⁸:

$$Q_i = \tilde{q}FL(1 - \text{RH}), \quad (1)$$

where RH is the ambient relative humidity and F a geometrical factor. \tilde{q} is related to the solubility and diffusivity of water in PDMS and of the order of $\tilde{q} \simeq 0.5 \mu\text{m}^2 \text{s}^{-1}$ ^{32-34,38,39}. Since \tilde{q} is an intrinsic parameter of PDMS, the only possible optimisation in our application is geometric (F and L).

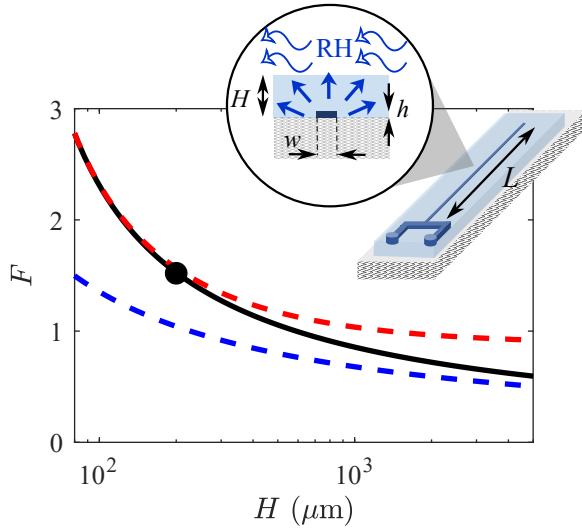


FIG. 4. Schematic perspective and sectional views of a single channel in a PDMS chip. Geometrical factor F in eqn 1 for the case $h = 30 \mu\text{m}$ and $w = 50 \mu\text{m}$ calculated by Dollet *et al.*³⁸. The red dotted line is eqn S2 which correctly approximates the analytical solution for $H \leq 200 \mu\text{m}$. The blue dotted line is eqn S1 which roughly approximates the case of a thick chip. The black dot indicates the value $F \simeq 1.5$ for $H = 200 \mu\text{m}$.

Dollet *et al.* also provided exact analytical solutions for F using conformal-mapping techniques for a channel with rectangular cross-section³⁸. Fig. 4 shows this calculation (as well as approximations detailed in Supplementary Information, Sec. S2) for the case $h = 30$, $w = 50 \mu\text{m}$ and various thicknesses H . These calculations show that the geometrical factor increases only moderately from $F \simeq 0.6$ for $H = 5 \text{ mm}$ to $F \simeq 2.3$ for a $H = 100 \mu\text{m}$ thin chip. Higher factors could be achieved for thinner chips (because of the divergent term in eqn S2 when $H \rightarrow h$), but the handling of thin cm^2 PDMS layers in the microfabrication stages remains tricky, and we found that $H \simeq 200 \mu\text{m}$ is a good compromise ($F \simeq 1.5$). Such thicknesses lead to pervaporation-driven flow rates of the order of $Q_i \simeq 0.1 \mu\text{L h}^{-1}$ assuming $\tilde{q} \simeq 0.5 \mu\text{m}^2 \text{s}^{-1}$ and

a $L = 4 \text{ cm}$ centimetre long channel (at $\text{RH} = 0$). As we will see later, such flow rates are too low for the proof of concept of EK energy conversion targeted by our study.

To reach much higher flow rates, the dead-end channels need to be parallelized in a single chip, as is the case for the venation of real leaves, see Fig. 5(a) showing N parallel channels connected to the same inlet. This configuration has been

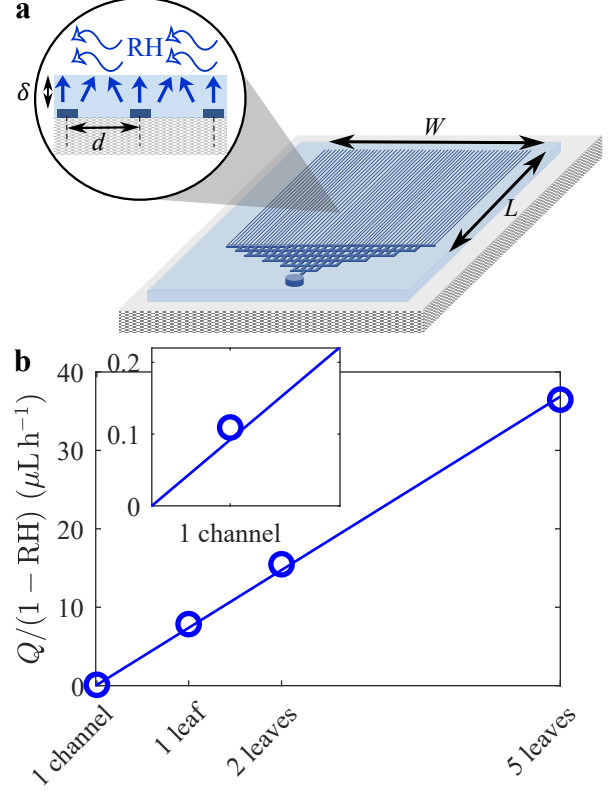


FIG. 5. (a) Schematic perspective and sectional views of the PDMS leaf. The channels have a rectangular cross-section $h \times w$ and $\delta = H - h$, H being the thickness of the PDMS layer. (b) Measured flow rate Q achieved using multiple leaves placed in parallel. Q is rescaled by $1 - \text{RH}$ (RH varied from 0.4 to 0.5 in these experiments). The 1-channel case corresponds to the theoretical estimation of eqn 1 for $H = 200 \mu\text{m}$, and is also shown in the inset. The continuous line is a linear fit.

studied by Noblin *et al.*³⁵ who showed that the overall pervaporation rate follows $Q = NQ_i$ for small channel density $1/d \ll 1/H$, but saturates for higher density to the limiting value:

$$Q_{\text{lim}} \simeq \frac{LW}{\delta} \tilde{q}(1 - \text{RH}). \quad (2)$$

This regime is due to the screening of the diffusion of water in the PDMS matrix between the channels and corresponds to the 1D pervaporation through a PDMS layer of thickness $\delta = H - h$. This effect is similar to the screening of evaporation from a network of pores, as in the case of the stomata of real leaves^{31,40}, or as for nanoporous media in the context of EK energy harvesting⁴¹. The experimental case studied in this work, $N = 79$ parallel channels in a $W = 3.9 \text{ cm}$ wide leaf,

lies a priori between these two regimes because $d = 500 \mu\text{m}$ is close to $H = 200 \mu\text{m}$. We thus used numerical resolutions detailed in Supplementary Information, see Fig. S2 and S3, to show that the pervaporation-driven flow rate in our case is given by $Q = \alpha Q_{\text{lim}}$ with $\alpha \simeq 0.5$.

Fig. 5(b) reports the measurements of the flow rate Q induced by pervaporation of water from 1, 2, and 5 PDMS leaves connected in parallel. In these experiments, the leaves are gently filled with pure water by imposing an inlet pressure of between 1 to 3 bar, to completely remove the air initially present in the dead-end channels. The flow rate Q is then measured thanks to a flowmeter upstream of the leaves, and rescaled by $1 - \text{RH}$ to account for the variations of the ambient conditions (temperature range $\simeq 20\text{--}22^\circ\text{C}$, $\text{RH} = 0.4\text{--}0.5$). Our data show a linear scaling of $Q/(1 - \text{RH})$ with the pervaporation area as expected from theory. The linear fit in Fig. 5(b) together with eqn 2 and the prefactor $\alpha \simeq 0.5$ estimated numerically leads to $\tilde{q} \simeq 0.4 \mu\text{m}^2\text{s}^{-1}$ in agreement with the reported values so far^{32–34,38,39}. The maximal rate measured of the order of $Q \simeq 18 \mu\text{L h}^{-1}$ for the 5-leaves case at $\text{RH} = 0.5$, corresponds a $\simeq 350$ -fold increase of the single channel case. As demonstrated later in this work, such values are now compatible with the proof of concept of EK conversion from pervaporation-driven flows.

The 1D description of eqn 2 leads to the pervaporation flux per unit surface $J_p = \alpha \tilde{q}(1 - \text{RH})/\delta$, which can be compared to the water evaporation flux J_e from a free surface, or equivalently from a dense array of nanopores^{29,41}. The later is given by $\rho_w J_e \simeq D_w^{\text{air}} C_{\text{sat}}^{\text{air}}(1 - \text{RH})/l$, ρ_w (kg m^{-3}) being the density of liquid water, $C_{\text{sat}}^{\text{air}}$ (kg m^{-3}) the water concentration in the gas phase at saturation, D_w^{air} (m^2s^{-1}) the diffusion coefficient of water as vapor in the gas phase, and l the thickness of the stagnant boundary layer. For $l \simeq 2 \text{ mm}$, typical for moderate air convection over a surface area of a few square centimetres²⁹, $J_e \simeq 200 \text{ nm s}^{-1}$ for ambient conditions ($\text{RH} = 0.5$) while $J_p \simeq 1 \text{ nm s}^{-1}$. $J_p \ll J_e$ is in line with the low water permeability of PDMS, and also demonstrates that the measured pervaporation rates shown in Fig. 5(b) do not depend on the air convection around the leaves, as the overall mass transfer is limited by the pervaporation through the PDMS matrix (resistance $\mathcal{R}_{\text{PDMS}} = \delta/(\alpha \tilde{q})$) and not by mass transfer in air (resistance $\mathcal{R}_{\text{air}} = \rho_w l / (D_w^{\text{air}} C_{\text{sat}}^{\text{air}}) \ll \mathcal{R}_{\text{PDMS}}$).

For a single leaf, the flow rate $Q \simeq 3.9 \mu\text{L h}^{-1}$ for $\text{RH} = 0.5$ (see Fig. 5(b)) is associated with an emptying time of the channel network of the order of $\tau_p \simeq NwLh/Q \simeq 70 \text{ min}$. Pervaporation therefore induces water flows with an average velocity $V_p \simeq L/\tau_p \simeq 9 \mu\text{m s}^{-1}$ at the entrance of each channel, decreasing linearly to 0 at their end according to mass conservation³⁸. This flow inevitably leads to a continuous accumulation in the microfluidic channels of all the solutes that are insoluble in the PDMS matrix (e.g., salts), as also observed in the context of evaporation-driven electrokinetic energy conversion in microfluidic glass channels¹⁹, see also Ref.³⁴. Because of the balance between pervaporation-driven advection and solute diffusion, the concentration of solutes only increases at the tip of the channels in a volume $\simeq pwh$, with $p \simeq \sqrt{D_s \tau_p}$ (D_s being the solute diffusion coefficient) and at a rate $p\dot{C} \simeq V_p c_s$, with c_s the solute concentration at

the entrance of the channel, see Ref.³⁴ for details. For salts at a concentration $c_s = 0.1 \text{ mM}$, $D_s \simeq 10^{-9} \text{ m}^2\text{s}^{-1}$, $p \simeq 2 \text{ mm}$, and the salt concentration at the tip is expected to reach $\simeq 1 \text{ M}$ only after few weeks, so we can state that the accumulation of solutes induced by pervaporation in the experiments described in Sec. III C does not affect the leaf pervaporation rates (see Ref.³⁴ for more informations).

B. Characterisation of the EK conversion element

As our aim is to harvest measurable electrical power from pervaporation-driven flows at relatively low rates ($Q < 20 \mu\text{L h}^{-1}$), it is necessary for the EK conversion element to have a hydraulic resistance R_h which results in a non-negligible pressure drop $\Delta P = R_h Q$ and mechanical power $\mathcal{P}_h = \Delta P Q$. The hydraulic resistance of a colloid plug in a tube of inner diameter $2R_t$ as shown in Fig. 3(a) can be estimated by:

$$R_h = \frac{\eta_w L_p}{\pi R_t^2 \kappa_{\text{CK}}}, \quad (3)$$

η_w being the viscosity of water and $\kappa_{\text{CK}} \simeq 5.7 \times 10^{-15} \text{ m}^2$ the hydraulic permeability estimated by the Carman-Koseny relation $\kappa_{\text{CK}} = a^2(1 - \phi_d)^3/(45\phi_d^2)$, assuming random close-packing, i.e., $\phi_d = 0.64$. This simple estimate leads to a length L_p of a few cm in a tube with $R_t = 0.5 \text{ mm}$ to achieve a pressure drop of the order of $\Delta P \sim 1 \text{ bar}$ for flows driven by pervaporation in the PDMS leaves described previously (Fig. 5).

Fig. 6(a) shows the measurements of the steady state flow rate Q across a colloidal plug of length $L_p \simeq 2 \text{ cm}$ in a tube radius $R_t = 0.5 \text{ mm}$, resulting from imposed pressure drops in the range $\Delta P = [0\text{--}6] \text{ bar}$. The linear behaviour $\Delta P = R_h Q$ with $R_h \simeq 1 \text{ bar min } \mu\text{L}^{-1}$, demonstrates that the plug of colloids does not significantly deform up to 6 bar and simply acts as a hydraulic resistance, and eqn 3 leads to $\kappa_t \simeq 4 \times 10^{-15} \text{ m}^2$ close to the Carman-Koseny estimate given above. Note that we also confirmed in separate experiments without the colloid plug, that R_h largely dominates the resistance R_f of the filter, tubes, and the connectors, of the order of $R_f \approx 1 \times 10^{-3} \text{ bar min } \mu\text{L}^{-1}$.

Fig. 3(b) shows the equivalent electrical circuit of the EK conversion element⁴ connected to a primary conditioning circuit composed of a variable load resistance R_L . A pressure-driven flow through the interstices of the colloid plug generates a streaming current $S_{\text{str}} \Delta P$, S_{str} (A bar^{-1}) being the streaming conductance of the EK conversion element. A fraction I of this current is collected in the external resistance R_L , and the other part corresponds to the electro-migration current through the EK conversion element (of electric resistance R_C) due to the streaming potential V . In this classic description, V and ΔP are related by:

$$V = \frac{R_C R_L}{R_C + R_L} S_{\text{str}} \Delta P, \quad (4)$$

and the electrical power harvested $\mathcal{P}_e = VI$ is maximal for $R_L = R_C$ ⁴. Fig. 6(b) reports the measurements of the streaming potential V for a NaCl aqueous solution at concentration

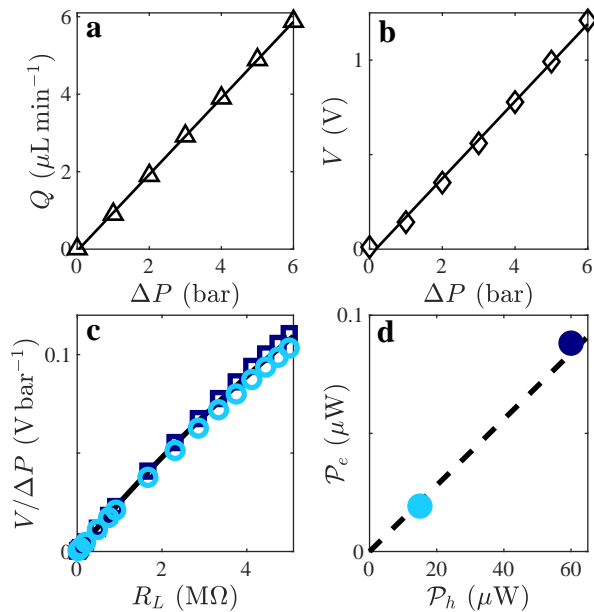


FIG. 6. Characterisation of the EK conversion element. (a) Flow rate Q across the colloidal plug and (b) streaming potential V for $R_L = 10 \text{ M}\Omega$, as a function of the imposed pressure drop ΔP . The continuous lines are linear fits. (c) Streaming potential V (normalised by ΔP) as a function of the load resistance R_L (\circ light blue: $\Delta P = 3 \text{ bar}$, \square dark blue: $\Delta P = 6 \text{ bar}$). The continuous line is the best fit by eqn 4, see text. (d) Electrical output power \mathcal{P}_e at $R_L = 5 \text{ M}\Omega$ against the mechanical power \mathcal{P}_h . The dotted line shows an efficiency $\varepsilon \simeq 0.14\%$. In these experiments, $L_p \approx 2 \text{ cm}$, $R_t = 0.5 \text{ mm}$, and the NaCl concentration is $c_s = 0.1 \text{ mM}$.

$c_s = 0.1 \text{ mM}$, as a function of the imposed pressure drop ΔP and for $R_L = 10 \text{ M}\Omega$ (the maximal value of the R_L tested, corresponding to the internal impedance of the multi-meter we used, see Sec. II B). The linear behaviour $V \propto \Delta P$ is expected from eqn 4, and our measurements show that the EK conversion element is able to generate a streaming potential of $V \simeq 1 \text{ V}$ for a pressure drop $\Delta P \simeq 5 \text{ bar}$. Fig. 6(c) now shows $V/\Delta P$ as a function of R_L and for two imposed pressure drops, $\Delta P = 3$ and 6 bar . The collapse is expected from eqn 4 and the best fit leads to $S_{\text{str}} \simeq 25 \text{ nA bar}^{-1}$ and $R_C \simeq 25 \pm 5 \text{ M}\Omega$. The estimated value of R_C is associated with a significant uncertainty since $R_L < R_C$ in our configuration. The choice of the salt concentration $c_s = 0.1 \text{ mM}$ comes from experiments similar to those described in Fig. 6 but for $c_s = 0.01$ and $c_s = 1 \text{ mM}$, leading to lower streaming conductances (data not shown). Such a concentration value is also in agreement with the optimal concentration found in experiments on model nanofluidic channels⁴ whose dimensions are a priori close to those of the interstices of our porous medium.

Fig. 6(d) finally shows the harvested electric power $\mathcal{P}_e = V^2/R_L$ as a function of the input mechanical power $\mathcal{P}_h = \Delta P Q$ for $R_L = 5 \text{ M}\Omega$ (corresponding thus to $R_{\text{var}} = R_{\text{app}}$, see Sec. II B). These data show that the maximal power generated at $\Delta P = 6 \text{ bar}$ is about $\mathcal{P}_e \simeq 0.09 \text{ }\mu\text{W}$ and the linear relation $\mathcal{P}_e = \varepsilon \mathcal{P}_h$ indicates an EK conversion efficiency of $\varepsilon \simeq 0.14\%$, while efficiencies up to 3% have been re-

ported using nanofluidic channels⁴ and up to 1.3% using a glass microchannel array⁶. Note that in our configuration, $R_L < R_C$ due to the use of a standard multi-meter with internal impedance which imposes a maximal load resistance of $R_L = 10 \text{ M}\Omega$. We are thus not fully exploiting the efficiency of the EK conversion element, which should be at its maximum for $R_L = R_C \simeq 25 \text{ M}\Omega$. However, we have confirmed the validity of eqn 4 by carrying out similar experiments but for a colloid plug of length $L_p \simeq 3 \text{ mm}$ and hydraulic resistance $R_h \simeq 0.11 \text{ bar min } \mu\text{L}^{-1}$, see Fig. S4. These measurements led this time to an internal resistance $R_C \simeq 4.1 \text{ M}\Omega$ and the harvested electric power reaches a maximum for $R_L = R_C$, associated to an efficiency of $\varepsilon \simeq 0.18\%$. However, such a device would not make it possible to achieve significant pressure drops ΔP for the proof of concept targeted by our study because the hydraulic resistance is 9 times lower than that characterised in Fig. 6(a).

In the following sections, we do not seek to maximise the conversion efficiency ε by exploring factors such as the nature and size of the colloids, or by maximising the collection of the streaming current by the electrodes (also affecting ε ^{6,29,36}). Instead, we focus on the increase of the harvested EK energy \mathcal{P}_e through the increase in input mechanical energy $\mathcal{P}_h = \Delta P Q$ (with leaves imposing a flow rate Q , and the EK conversion element imposing a pressure drop ΔP), and the limitations of this configuration due to cavitation.

C. Pervaporation-driven electrokinetic energy harvesting

We now discuss the coupling of the PDMS leaves described in Sec. III A with the EK conversion element characterized in Sec. III B. In such experiments, we first imposed a pressure of 8 bar on a reservoir of a NaCl solution ($c_s = 0.1 \text{ mM}$) upstream of the EK conversion element, and we plugged the downstream tube to 1 up to 5 leaves in parallel. Once the leaves are completely filled (no air bubbles trapped in the channels), the flow rate Q is driven only by water pervaporation because the channels have no outlets, and we released the reservoir to the atmospheric pressure. We then measured the streaming potential V over the load resistance R_L placed in parallel of the EK conversion element, to estimate the electric power $\mathcal{P}_e = V^2/R_L$, see Fig. 2.

Fig. 7(a) shows the measured data $V/\Delta P$ vs. R_L , for flows driven by water pervaporation in 1, 2, and 5 PDMS leaves in parallel. The pressure drop ΔP across the EK conversion element is estimated using its hydraulic resistance R_h (Fig. 6(a)) and the measured flow rates Q (Fig. 5(b)), and varied from $\Delta P = R_h Q \simeq 0.07 \text{ bar}$ for one leaf, to $\Delta P \simeq 0.32 \text{ bar}$ for 5 leaves. All the data $V/\Delta P$ against R_L almost collapse on a single curve (despite some dispersion due to the low currents) following again eqn 4 with the same parameters to those plotted in Fig. 6(c) when characterizing the EK conversion element by imposing mechanically a pressure drop. This shows that the same mechanisms are at play when the flow is imposed mechanically or driven passively by pervaporation.

Fig. 7(b) now reports the output electrical power \mathcal{P}_e generated by the pervaporation-driven flows for $R_L = 5 \text{ M}\Omega$, against

the mechanical power $\mathcal{P}_h = \Delta P Q$. Although the values of \mathcal{P}_e are small, they are measurable and reach $\mathcal{P}_e \simeq 0.18$ nW for the 5-leaves case. The linear fit shown in Fig. 7(b) corresponding to the efficiency $\varepsilon = \mathcal{P}_e / \mathcal{P}_h \simeq 0.14\%$ found previously (Fig. 6(d)), approximates the experimental data. It should be

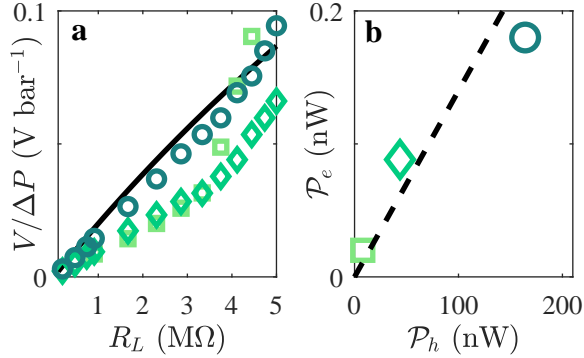


FIG. 7. Pervaporation-driven EK energy harvesting. (a) Streaming potential V normalised by the pressure drop ΔP as a function of the load resistance R_L , the flow is driven by water pervaporation in 1 (\square , light green), 2 (\diamond , green) and 5 (\circ , dark green) PDMS leaves placed in parallel. The continuous line is eqn 4 with the same parameters as in Fig. 6(c). (b) Corresponding generated electrical power $\mathcal{P}_e = V^2/R_L$ for $R_L = 5$ $\text{M}\Omega$, against the input mechanical power \mathcal{P}_h . The dotted line is the linear relation with $\varepsilon = 0.14\%$ also found in Fig. 6(d). In these experiments, $L_p \approx 2$ cm, $R_t = 0.5$ mm, and the NaCl concentration is $c_s = 0.1$ mM.

noted that such ε measurements have rarely been carried out in the case of evaporation-driven energy harvesting, as this measurement requires not only knowledge of the flow rate of evaporated water, but also the associated pressure drop across the element enabling EK energy conversion. As mentioned above, the low electrical power output is closely linked to the low permeability of water through PDMS, but it could also be increased by optimising the collection of the streaming currents by the electrodes, and the nature and size of the colloidal particles used. Nevertheless, the results in Fig. 7 provide the first experimental evidence of EK energy conversion from pervaporation-driven flows in PDMS chips.

D. Pervaporation-induced cavitation in the PDMS leaf

Fig. 7 shows that the configuration in which the EK conversion element is in series with the flow-driving element offers the possibility pointed out by Yaroshchuk²⁹ of increasing the output power simply by increasing, in our case, the pervaporation surface area. However, increasing the output power $\mathcal{P}_e = \varepsilon R_h Q^2$ in a passive system by increasing Q can also be limited by water cavitation caused by a large pressure drop $\Delta P = R_h Q$. This is illustrated in Fig. 8 in the case of a single leaf. Since the hydraulic resistance R_h of the colloidal plug is much larger than the other hydraulic resistances, including those of the channel network, the pressure in the leaf P_{leaf} , is

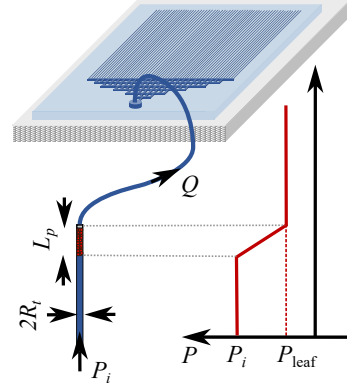


FIG. 8. The pressure drop ΔP due to the pervaporation-driven flow rate Q through the colloidal plug leads to a water pressure in the leaf P_{leaf} given by eqn 5. P_i is the pressure upstream of the plug.

almost uniform for the flow rates investigated, and given by:

$$P_{\text{leaf}} \simeq P_i - R_h Q, \quad (5)$$

where P_i is the pressure upstream of the EK conversion element. In the data shown in Fig. 7, the water reservoir is opened to the atmospheric pressure ($P_i \simeq 1$ bar) and we found $\Delta P \simeq 0.3$ bar for the 5-leaves case, leading thus to $P_{\text{leaf}} \simeq 0.7$ bar, significantly smaller than P_i but still positive.

To test the possible cavitation of water for negative leaf pressures, we performed the experiment detailed below and shown in Fig. 8. We first imposed a flow of water with a pressure $P_i = 8$ bar through a colloid plug of length $L_p \simeq 6$ cm in a tube of inner radius $R_t \simeq 0.125$ mm, while measuring simultaneously the resulting flow rate Q . This leads to an estimate of the hydrodynamic resistance of the plug, $R_h \simeq 33$ bar $\text{min } \mu\text{L}^{-1}$, and eqn 3 gives a permeability $\kappa_h \simeq 5.9 \times 10^{-15}$ m^2 , close to the Carman-Koseny estimate κ_{CK} (see Sec. III B). While still imposing $P_i = 8$ bar, the tube downstream of the plug is connected to a PDMS leaf ($H = 200$ μm). Once the air trapped in the dead-end channels have fully permeated through the PDMS layer, the flow rate Q (now driven only by pervaporation) reaches $Q \simeq 9$ $\mu\text{L h}^{-1}$ after a transient ($t > 30$ min, see Fig. 9). This steady value is then used in eqn 5 to estimate the leaf pressure $P_{\text{leaf}} \simeq 3$ bar, see the inset of Fig. 9 showing the data Q vs. P_{leaf} .

At $t = 120$ min, we then imposed lower inlet pressure levels lasting 2 h, while simultaneously monitoring the channel network using microscopy at an acquisition frequency of one image every two minutes (Movie S1 in Supplementary information). For each level of imposed P_i , we observed a temporal relaxation of the flow rate to a steady value, which is again used to estimate the leaf pressure with eqn 5. For $P_{\text{leaf}} > 0$, the steady pervaporation-driven flow rates vary with P_{leaf} decreasing from $Q \simeq 9$ $\mu\text{L h}^{-1}$ at $P_{\text{leaf}} \simeq 3$ bar to a constant value $Q \simeq 4$ $\mu\text{L h}^{-1}$ for $P_{\text{leaf}} \leq 2$ bar. This variation is actually due to the mechanical deformation of the PDMS layer for high leaf pressures (visible at high magnification), affecting notably the transverse dimensions of both the channel network and the PDMS layer, and thus the pervaporation-driven flow

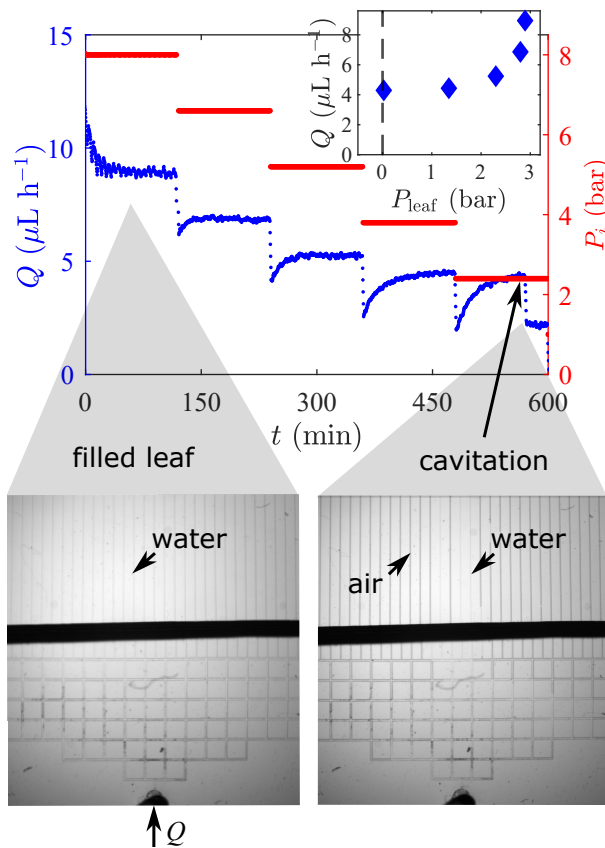


FIG. 9. Pervaporation-induced cavitation in a PDMS leaf. Flow rates Q vs. time t (left axis, blue) measured for different levels of imposed pressure P_i (right axis, red). The inset shows the flow rate value Q at steady state against the pressure in the leaf estimated using eqn 5. For $t < 570$ min, the leaf is filled and water pervaporation induces a flow (bottom left image). At $t = 570$ min, cavitation occurs in the leaf leading to the formation of bubbles that stop the pervaporation-driven flow (bottom right image), see also Movie S1 in Supplementary information.

rate Q . We confirmed this hypothesis by measuring Q for a PDMS leaf directly connected to a pressure controller to impose P_{leaf} (data not shown). These mechanical deformations of the PDMS leaf also explain the poro-elastic relaxations of the measured flow rate Q at each change in the level of imposed P_i , as can be seen in Fig. 9.

Interestingly, for $P_i = 2.4$ bar ($t > 480$ min), the flow rate first increases up to $Q \simeq 4.3 \mu\text{L h}^{-1}$ corresponding to a leaf pressure $P_{\text{leaf}} \simeq 0$ bar. Then, cavitation occurs suddenly at $t \simeq 570$ min resulting in the formation of bubbles in the PDMS leaf, and stopping the pervaporation-driven flow (see the sudden drop in the measured Q in Fig. 9). We repeated this experiment several times with different leaves, but we always observed cavitation for $P_{\text{leaf}} \simeq 0$ bar. This result is in contradiction with the experiments of Bruning *et al.* who reported a cavitation threshold $P_{\text{cap}} \simeq -13$ bar, but for a drying water droplet initially trapped in a PDMS mixture during its cross-linking, thus resulting in a defect-free cavity⁴². We thus believe that our observations of systematic cavitation at

$P_{\text{leaf}} \simeq 0$ bar, is due both to the hydrophobic nature of PDMS and to the defects due to typical microfabrication processes that can trap precursors of heterogeneous cavitation^{43,44}, despite the initial pressure level at $P_{\text{leaf}} \simeq 3$ bar for 2 h (Fig. 9) that should eliminate some of the air nanobubbles trapped in the channels.

IV. CONCLUSION

In the present work, we designed a simple device combining PDMS microfluidic chips and a plug of colloids closely-packed in a tube to provide the first evidence of EK energy harvesting from pervaporation-driven flows. Although the output electric powers \mathcal{P}_e are low, we have shown that it is possible to achieve higher \mathcal{P}_e simply by increasing the evaporation surface area, and thus the passively-driven flow rate Q .

The versatility and simplicity of the device we have developed offer multiple possibilities for optimisation, in particular by screening for different colloids in the EK conversion element, but also for the ionic strength of the input solution. Furthermore, the development of hydrogel-based microfluidic chips should make it possible to achieve much higher electrical powers, thanks to the greater water permeability of these materials compared to PDMS, and the rules discussed in Sec. III A for designing the channel network of the artificial leaves should also apply in these cases. It should be noted, however, that unlike PDMS, the overall EK energy harvesting performance of hydrogel-based leaves could then be affected by air convection due to their high water permeability.

In our work, we have also demonstrated that EK energy harvesting is limited for high pervaporation-driven flow rates by water cavitation, which systematically occurs when the pressure drop reaches $\Delta P = R_h Q \simeq 1$ bar corresponding to a water pressure in the PDMS leaves of $P_{\text{leaf}} = P_{\text{cav}} \simeq 0$ bar. To significantly reduce the cavitation threshold P_{cav} in the leaves, it is necessary to use hydrophilic materials, unlike PDMS, and to avoid the presence of surface defects that could trap cavitation precursors^{43,44}. Hydrogel-based chips are possibly good candidates because these materials are intrinsically hydrophilic, and stable flows at significantly negative water pressures (down to $P_{\text{cav}} = -16.7$ bar) have been reported despite the inevitable presence of defects due to the microfabrication process^{18,45}. It is important to note that, regardless of the cavitation threshold P_{cav} in the element driving the water flow, cavitation a priori always limits the efficiency of the EK energy harvesting in such passive systems as the maximum flow rate cannot exceed $Q = P_{\text{cav}}/R_h$. This intrinsic limit has never been observed when water evaporation occurs directly from a saturated porous EK energy conversion element, likely due to the very high confinement of water in this case. It is instead capillary phenomena that limit energy harvesting in such configurations, since a too large pressure drop can lead to a receding of the evaporation surface within the conversion element²⁹, possibly also coupled to the Kelvin effect in the case of nanopores⁴⁶.

Beyond the application studied in the present work, the cav-

itation threshold measured in the PDMS leaf, together with the variations of the pervaporation-driven flow rate with the applied pressure deforming the channels (see Fig. 9) were not reported to our knowledge and could be of interest for the biomimetic studies exploiting pervaporation in PDMS microfluidic chips to study air propagation in plant leaves after cavitation and embolism formation^{47,48}.

ACKNOWLEDGEMENTS

This study received financial support from the French government in the framework of the University of Bordeaux's IdEx "Investments for the Future" program/ GPR PPM. We would like to thank G. Clisson for his technical assistance with the microfluidic experiments, O. Vincent for discussions on heterogeneous cavitation, A. L. Biance and C. Ybert for discussions of electrokinetic phenomena.

- 1 J. F. Osterle, "Electrokinetic Energy Conversion," *J. Appl. Mech.* **31**, 161 (1964).
- 2 W. Olthuis, B. Schippers, J. Eijkel, and A. Van Den Berg, "Energy from streaming current and potential," *Sens. Actuators, B* **111**, 385 (2005).
- 3 M.-C. Lu, S. Satyanarayana, R. Karnik, A. Majumdar, and C.-C. Wang, "A mechanical-electrokinetic battery using a nano-porous membrane," *J. Micromech. Microeng.* **16**, 667 (2006).
- 4 F. H. Van Der Heyden, D. J. Bonthuis, D. Stein, C. Meyer, and C. Dekker, "Power generation by pressure-driven transport of ions in nanofluidic channels," *Nano Lett.* **7**, 1022 (2007).
- 5 F. H. J. Van Der Heyden, D. J. Bonthuis, D. Stein, C. Meyer, and C. Dekker, "Electrokinetic Energy Conversion Efficiency in Nanofluidic Channels," *Nano Lett.* **6**, 2232 (2006).
- 6 A. Mansouri, S. Bhattacharjee, and L. Kostiuk, "High-power electrokinetic energy conversion in a glass microchannel array," *Lab Chip* **12**, 4033 (2012).
- 7 J. Zhang, K. Zhan, S. Wang, and X. Hou, "Soft interface design for electrokinetic energy conversion," *Soft Matter* **16**, 2915 (2020).
- 8 C. Li, K. Liu, H. Liu, B. Yang, and X. Hu, "Capillary driven electrokinetic generator for environmental energy harvesting," *Mater. Res. Bull.* **90**, 81 (2017).
- 9 G. Xue, Y. Xu, T. Ding, J. Li, J. Yin, W. Fei, Y. Cao, J. Yu, L. Yuan, L. Gong, J. Chen, S. Deng, J. Zhou, and W. Guo, "Water-evaporation-induced electricity with nanostructured carbon materials," *Nat. Nanotechnol.* **12**, 317 (2017).
- 10 X. Liu, H. Gao, J. E. Ward, X. Liu, B. Yin, T. Fu, J. Chen, D. R. Lovley, and J. Yao, *Nature* **578**, 550 (2020).
- 11 X. Liu, T. Ueki, H. Gao, T. L. Woodard, K. P. Nevin, T. Fu, S. Fu, L. Sun, D. R. Lovley, and J. Yao, "Microbial biofilms for electricity generation from water evaporation and power to wearables," *Nat. Commun.* **13**, 1 (2022).
- 12 D. Shen, W. W. Duley, P. Peng, M. Xiao, J. Feng, L. Liu, G. Zou, and Y. N. Zhou, "Moisture-Enabled Electricity Generation: From Physics and Materials to Self-Powered Applications," *Adv. Mater.* **32**, 2003722 (2020).
- 13 A. H. Cavusoglu, X. Chen, P. Gentine, and O. Sahin, "Potential for natural evaporation as a reliable renewable energy resource," *Nat. Commun.* **8**, 617 (2017).
- 14 Z. Zhang, X. Li, J. Yin, Y. Xu, W. Fei, M. Xue, Q. Wang, J. Zhou, and W. Guo, "Emerging hydrovoltaic technology," *Nat. Nanotechnol.* **13**, 1109 (2018).
- 15 S. S. Das, S. Kar, T. Anwar, P. Saha, and S. Chakraborty, "Hydroelectric power plant on a paper strip," *Lab Chip* **18**, 1560 (2018).
- 16 S. S. Das, V. M. Pedireddi, A. Bandopadhyay, P. Saha, and S. Chakraborty, "Electrical Power Generation from Wet Textile Mediated by Spontaneous Nanoscale Evaporation," *Nano Lett.* **19**, 7191 (2019).
- 17 K. Saha, J. Deka, and K. Raidongia, "Extraction of Evaporation-Driven Electrokinetic Streaming Potential from V2O5 Nanochannels through Secondary Sources," *ACS Appl. Energy Mater.* **4**, 8410 (2021).
- 18 Y. Liu, Z. Yu, X. Liu, P. Cheng, Y. Zhao, Y. Ma, P. Yang, and K. Liu, "Negative Pressure in Water for Efficient Heat Utilization and Transfer," *Nano Lett.* **23**, 6651 (2023).
- 19 N. Yanagisawa, V. Dominguez, S. Mahmud, and D. Dutta, "Characterization of liquid flow and electricity generation in a glass channel based evaporation-driven electrokinetic energy conversion device," *Phys. Fluids* **35**, 053604 (2023).
- 20 B. R. Bora, N. Nath, M. Dey, K. Saha, and K. Raidongia, "Assembly of Natural Clay Minerals as Highly Robust Evaporation-Driven Power Generator," *ACS Appl. Energy Mater.* **7**, 6507 (2024).
- 21 K. Jiao, H. Yan, F. Qian, W. Zhang, H. Li, Q. Wang, and C. Zhao, "Energy harvesting based on water evaporation-induced electrokinetic streaming potential/current in porous carbonized carrots," *J. Power Sources* **569**, 233007 (2023).
- 22 T. Ding, K. Liu, J. Li, G. Xue, Q. Chen, L. Huang, B. Hu, and J. Zhou, "All-Printed Porous Carbon Film for Electricity Generation from Evaporation-Driven Water Flow," *Adv. Funct. Mater.* **27**, 1700551 (2017).
- 23 G. Zhang, Z. Duan, X. Qi, Y. Xu, L. Li, W. Ma, H. Zhang, C. Liu, and W. Yao, "Harvesting environment energy from water-evaporation over free-standing graphene oxide sponges," *Carbon* **148**, 1 (2019).
- 24 T. G. Yun, J. Bae, A. Rothschild, and I. D. Kim, "Transpiration Driven Electrokinetic Power Generator," *ACS Nano* **13**, 12703 (2019).
- 25 J. Bae, T. G. Yun, B. L. Suh, J. Kim, and I. D. Kim, "Self-operating transpiration-driven electrokinetic power generator with an artificial hydrological cycle," *Energy Environ. Sci.* **13**, 527 (2020).
- 26 Y. Qin, Y. Wang, X. Sun, Y. Li, H. Xu, Y. Tan, Y. Li, T. Song, and B. Sun, "Constant Electricity Generation in Nanostructured Silicon by Evaporation-Driven Water Flow," *Angew. Chem., Int. Ed.* **59**, 10619 (2020).
- 27 J. Bae, M. S. Kim, T. Oh, B. L. Suh, T. G. Yun, S. Lee, K. Hur, Y. Gogotsi, C. M. Koo, and I. D. Kim, "Towards Watt-scale hydroelectric energy harvesting by Ti3C2TX-based transpiration-driven electrokinetic power generators," *Energy Environ. Sci.* **15**, 123 (2022).
- 28 A. T. Liu, G. Zhang, A. L. Cottrill, Y. Kunai, A. Kaplan, P. Liu, V. B. Koman, and M. S. Strano, "Direct Electricity Generation Mediated by Molecular Interactions with Low Dimensional Carbon Materials—A Mechanistic Perspective," *Adv. Energy Mater.* **8**, 1802212 (2018).
- 29 A. Yaroshchuk, "Evaporation-driven electrokinetic energy conversion: Critical review, parametric analysis and perspectives," *Adv. Colloid Interface Sci.* **305**, 102708 (2022).
- 30 A. D. Stroock, V. V. Pagay, M. A. Zwieniecki, and N. M. Holbrook, "The physicochemical hydrodynamics of vascular plants," *Annu. Rev. Fluid Mech.* **46**, 615 (2014).
- 31 K. H. Jensen, K. Berg-Sørensen, H. Bruus, N. M. Holbrook, J. Liesche, A. Schulz, M. A. Zwieniecki, and T. Bohr, "Sap flow and sugar transport in plants," *Rev. Mod. Phys.* **88**, 035007 (2016).
- 32 E. Verneuil, A. Buguin, and P. Silberzan, "Permeation-induced flows: Consequences for silicone-based microfluidics," *Europhys. Lett.* **68**, 412 (2004).
- 33 G. C. Randall and P. S. Doyle, "Permeation-driven flow in poly(dimethylsiloxane) microfluidic devices," *Proc. Natl. Acad. Sci. USA* **102**, 10813 (2005).
- 34 P. Bacchin, J. Leng, and J. B. Salmon, "Microfluidic Evaporation, Pervaporation, and Osmosis: From Passive Pumping to Solute Concentration," *Chem. Rev.* **122**, 6938 (2022).
- 35 X. Noblin, L. Mahadevan, I. A. Coomaraswamy, D. A. Weitz, N. M. Holbrook, and M. A. Zwieniecki, "Optimal vein density in artificial and real leaves," *Proc. Natl. Acad. Sci. USA* **105**, 9140 (2008).
- 36 K. Saha, J. Deka, and K. Raidongia, "Energy from the Nanofluidic Transport of Water through Nanochannels between Packed Silica Spheres," *ACS Appl. Nano Mater.* **2**, 5850 (2019).
- 37 Z. Chen, Y. Wang, W. Wang, and Z. Li, "Nanofluidic electrokinetics in nanoparticle crystal," *Appl. Phys. Lett.* **95**, 102105 (2009).
- 38 B. Dollet, J.-F. Louf, M. Alonzo, K. Jensen, and P. Marmottant, "Drying of channels by evaporation through a permeable medium," *J. R. Soc. Interface* **16**, 20180690 (2019).
- 39 S. J. Harley, E. A. Glascoe, and R. S. Maxwell, "Thermodynamic study on dynamic water vapor sorption in sylgard-184," *J. Phys. Chem. B* **116**, 14183 (2012).
- 40 P. Lehmann and D. Or, "Effects of stomata clustering on leaf gas exchange," *New Phytol.* **207**, 1015 (2015).

- ⁴¹A. Yaroshchuk and M. P. Bondarenko, "Interaction of Potential Sources in Infinite 2D Arrays: Diffusion through Composite Membranes, Micro-Electrochemistry, Entrance Resistance, and Other Examples," *Adv. Theory Simul.* **4**, 18 (2021).
- ⁴²M. A. Bruning, M. Costalonga, J. H. Snoeijer, and A. Marin, "Turning Drops into Bubbles: Cavitation by Vapor Diffusion through Elastic Networks," *Phys. Rev. Lett.* **123**, 214501 (2019).
- ⁴³O. Vincent, "Negative pressure and cavitation dynamics in plant-like structures," in *Soft Matter in Plants: From Biophysics to Biomimetics*, Soft Matter Series, edited by K. Jensen and Y. Forterre (Royal Society of Chemistry, 2022) p. 119.
- ⁴⁴P. Loche, M. Kanduc, E. Schneck, and R. R. Netz, "Water cavitation results from the kinetic competition of bulk, surface and surface-defect nucleation events," (2024), 2024, arXiv:2410.17626.
- ⁴⁵T. D. Wheeler and A. D. Stroock, "The transpiration of water at negative pressures in a synthetic tree," *Nature* **455**, 208 (2009).
- ⁴⁶O. Vincent, A. Szenicer, and A. D. Stroock, "Capillarity-driven flows at the continuum limit," *Soft Matter* **12**, 6656 (2016).
- ⁴⁷B. Dollet, K. N. Chagua Encarnación, R. Gautier, and P. Marmottant, "Drying by pervaporation in elementary channel networks," *J. Fluid Mech.* **906**, A6 (2021).
- ⁴⁸L. Keiser, P. Marmottant, and B. Dollet, "Intermittent air invasion in pervaporating compliant microchannels," *J. Fluid Mech.* **948**, A52 (2022).